

Probing Pseudo-Dirac Neutrinos with Astrophysical Sources at IceCube

Kiara Carloni,^{1,*} Ivan Martínez-Soler,^{1,†} Carlos A. Argüelles,^{1,‡} K. S. Babu,^{2,§} and P. S. Bhupal Dev^{3,¶}

¹*Department of Physics & Laboratory for Particle Physics and Cosmology,
Harvard University, Cambridge, MA 02138, USA*

²*Department of Physics, Oklahoma State University, Stillwater, OK 74078, USA*

³*Department of Physics and McDonnell Center for the Space Sciences,
Washington University, St. Louis, MO 63130, USA*

(Dated: April 17, 2023)

The recent observation of NGC 1068 by the IceCube Neutrino Observatory has opened a new window to neutrino physics with astrophysical baselines. In this *Letter*, we propose a new method to probe the nature of neutrino masses using these observations. In particular, our method enables searching for signatures of pseudo-Dirac neutrinos with mass-squared differences that reach down to $\delta m^2 \gtrsim 10^{-21} \text{eV}^2$, improving the reach of terrestrial experiments by more than a billion. Finally, we discuss how the discovery of a constellation of neutrino sources can further increase the sensitivity and cover a wider range of δm^2 values.

Introduction. — Since the beginning of time, humans have stared at the sky and wondered about the universe. Through careful inspection, we discovered the patterns that rule the motions of planets, and followed a trail of questioning that led to the theory of general relativity. Now, equipped with enormous telescopes and modern particle physics, we can, for the first time, study tinier, even more elusive astrophysical signals. In this *Letter*, we show that these observations can be used to uncover the origin and nature of the neutrino mass.

Recently, IceCube announced the observation of the first steady-state astrophysical neutrino source, the active galactic nucleus NGC 1068 [1, 2]. Assuming only that the neutrinos produced by this source follow a power-law distribution in energy, they performed a likelihood analysis and found that 79_{-20}^{+22} events originated from NGC 1068, yielding a rejection of the background-only hypothesis with a local (global) significance of 5.2 (4.2) σ [1]. Neutrinos that travel to Earth from sources like NGC 1068 must traverse megaparsecs (Mpc), a distance many orders of magnitude greater than that traveled by any solar, atmospheric, reactor- or accelerator-based neutrino ever detected. Therefore, exploring the properties of the neutrino events from extra-galactic sources will allow us to study, for the first time, a whole class of new physics scenarios whose signals appear only at extremely long length scales.

One significant example of such new physics is the pseudo-Dirac model of neutrino masses [3–6]. In this class of models, the active neutrino mass states are accompanied by undetectable sterile states, whose masses are separated from the active ones by a tiny amount, generated by a small Majorana mass term. The active-sterile mass splittings induce an oscillation between the active and sterile neutrino states. For very small Majorana masses, these oscillations are detectable only at extremely large values of the ratio L/E (where L is the baseline and E denotes the neutrino energy). These large values are achievable only for astrophysical neutrino

sources [7–13]. See Figure 1 for an artistic rendition of our main idea.

In this *Letter*, we explore how the pseudo-Dirac neutrino scenario could be probed by observations of extra-galactic neutrinos. We find that currently identified astrophysical neutrino sources can provide new constraints on yet unexplored mass splittings. We also predict how upcoming measurements in current and future neutrino telescopes will increase the sensitivity to these new mass splittings.

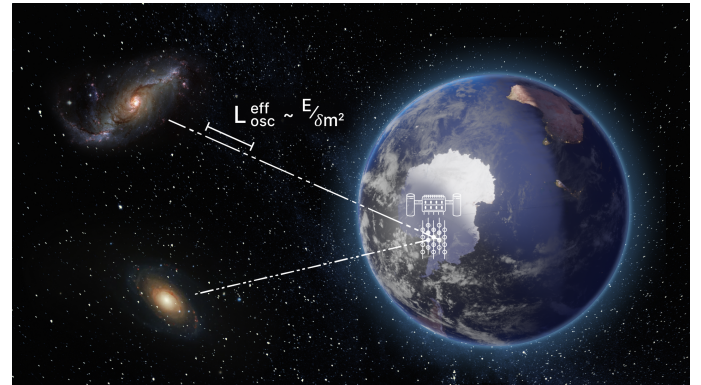


FIG. 1. An artistic rendering of neutrino propagation from extra-galactic sources. Oscillation from active to sterile is depicted by the transition from solid to dashed line.

Theory of pseudo-Dirac neutrinos. — Whether or not the neutrino is its own antiparticle is a question that is yet to be settled. In a wide class of beyond the Standard Model (BSM) theories, the neutrino is a Majorana fermion, which is its own antiparticle. However, there does exist a class of theories where the neutrino is a four-component Dirac fermion. Neutrino oscillation experiments are unable to distinguish its Majorana nature from a Dirac one. In this context, it is also possible that the neutrino is a *pseudo-Dirac particle* [3–6], which is fundamentally a Majorana fermion, but essentially acts like a Dirac fermion in most experimental settings. However,

they can be differentiated through active-sterile oscillations when the baseline traversed by the neutrino is extremely long relative to the detection energy.

The mass matrix spanning the active species ν_a and its Dirac partner ν_s has the form (with multiple flavors)

$$M_\nu = \begin{pmatrix} 0 & m_D \\ m_D^T & M_R \end{pmatrix}. \quad (1)$$

If $M_R = 0$ in Eq. (1), lepton number is preserved, and the neutrino is a Dirac particle; if $M_R \neq 0$, it is a Majorana particle; and if, in the eigenvalue sense, $|M_R| \ll |m_D|$, it is a pseudo-Dirac particle.

Phenomenologically, a pseudo-Dirac neutrino is one logical possibility in the context of neutrino mass generation. At first sight, the condition $|M_R| \ll |m_D|$ may not look natural since M_R is a gauge-invariant mass term in the SM, which could be much larger than the electroweak-symmetry-breaking scale, as e.g., in the original *seesaw mechanism* [14–17]. The smallness of the neutrino mass, compared to the charged fermion masses, would remain unexplained in this case of vanishing M_R . However, there are theories where M_D is naturally small and $M_R = 0$ at the renormalizable level. Nonzero elements of M_R are induced via higher-dimensional operators suppressed by the inverse Planck scale. This is the case in the *Dirac seesaw scenario* [18–23], which is realized naturally in the mirror universe model [24–26]. Such theories provide a better understanding of parity (P) violation, since P is an unbroken (or spontaneously broken) symmetry in this context. They provide mirror partners for every SM fermion, including lepton doublets $\Psi' = (\nu', \ell')$ of a mirror $SU(2)'_L$ symmetry which are the partners of the usual $SU(2)_L$ lepton doublet $\Psi = (\nu, \ell)$. In this context, ν' plays the role of sterile neutrinos, with its mass protected by the $SU(2)'_L$ gauge symmetry. A Dirac mass term connecting ν and ν' would arise from a generalized seesaw mechanism.

Operators of the type $(\Psi\Psi')(HH')/M_N$, where H and H' are the Higgs doublets of $SU(2)_L$ and mirror $SU(2)'_L$, respectively, are induced once a heavy neutral lepton N is integrated out. Specifically, N has interactions given by $(\Psi NH) + (\Psi' N' H') + (M_N/2)NN'$. Lepton number remains unbroken in this scenario, which also explains why the Dirac mass term $m_D = vv'/M_N$ (where v and v' are the vacuum expectation values of H and H' respectively) is very small. Alternatively, a bi-doublet Higgs $\Phi(2, 2)$ with the couplings $\Psi\Psi'\Phi + \mu HH'\Phi^*$ could lead to the same operator with a coefficient (μ/M_Φ^2) , once the Φ field is integrated out.

Now, quantum gravity corrections are expected to break all global symmetries, such as lepton number. One would then expect dimension-5 Weinberg operators [27] of the type $(\Psi\Psi HH)/M_{\text{Pl}}$ and $(\Psi'\Psi' H' H')/M_{\text{Pl}}$ would then be induced by gravity, with coefficients presumably of order unity. This would result in small diago-

nal entries of M_ν in Eq. (1), implying a pseudo-Dirac neutrino. In the mirror neutrino scenario, one would expect the active-sterile mass splitting to be on the order of $\delta m^2 \approx (2, 0.3) \times 10^{-7} \text{eV}^2$ (using $m_a \simeq (0.05, 0.007) \text{eV}$ for the larger two of the active neutrino masses with normal ordering). However, such mass splitting values are already excluded by solar neutrino data, which requires $\delta m^2 \lesssim 10^{-11} \text{eV}^2$ [28], with Ref. [29] finding a small preference for $\delta m^2 \simeq 1.2 \times 10^{-11} \text{eV}^2$.¹ This difficulty can be evaded by gauging the $B - L$ symmetry, which is anomaly-free in presence of sterile neutrinos. This gauge symmetry is spontaneously broken by a singlet scalar field, S , carrying two units of $B - L$ charge. The Weinberg operators would then be modified to the form $(\Psi\Psi HHS)/M_{\text{Pl}}^2$, leading to diagonal elements of M_ν on the order of $v^2 v_{BL}/M_{\text{Pl}}^2$. For the $B - L$ symmetry breaking scale of $v_{BL} = (10^4 - 10^{14}) \text{GeV}$ ² this would lead to a mass splitting of order $(10^{-22} - 10^{-12}) \text{eV}^2$. As we show below, a significant portion of this well-motivated range of v_{BL} would be probed by the high-energy neutrinos detected at IceCube. There are other models of naturally light Dirac neutrinos in the literature with tiny masses arising from quantum loop corrections, see e.g. Refs. [34–40]. Including Planck-suppressed higher-dimensional operators, many of these models would predict pseudo-Dirac neutrinos.

In all the pseudo-Dirac scenarios mentioned above, the mixing between active and sterile states, given by $\tan 2\theta = 2m_D/M_R$, is nearly maximal due to the pseudo-Dirac condition. The mass eigenstates of Eq. (1) are $\nu_S = \sin\theta \nu_a + \cos\theta \nu_s$ and $\nu_A = (-i)(\cos\theta \nu_a - \sin\theta \nu_s)$. For very large mixing angles, those states coincide with the symmetric ($\nu_S = (\nu_a + \nu_s)/\sqrt{2}$) and anti-symmetric ($\nu_A = -i(\nu_a - \nu_s)/\sqrt{2}$) combinations of the active and sterile neutrinos, with their mass difference being proportional to M_R .

The sterile component may have additional interactions with the SM fermions, such as of the form $\bar{\nu}_s^c \eta^+ \ell_R$, where η^+ is an $SU(2)_L$ -singlet charged scalar, which can be as light as $\sim 100 \text{GeV}$ and can induce a new Glashow-like resonance at IceCube [41, 42]. In this *Letter*, we will not consider this possibility and will focus on the minimal case where all the non-standard effects arise solely from the active-sterile neutrino mixing.

Neutrino evolution on astrophysical scales.— The neutrino flavor evolution is obtained by solving the Schrödinger equation along the neutrino trajectory. The time dependence of each flavor state is given by

¹ There also exist bounds on $\delta m^2 \lesssim 10^{-8} \text{eV}^2$ from Big Bang nucleosynthesis considerations [30, 31].

² $v_{BL} \lesssim 10^4 \text{GeV}$ is disfavored by the LHC null results on heavy Z' -resonance searches, assuming coupling strength similar to the weak interaction strength [32, 33].

$$|\nu_\alpha(t)\rangle = \exp\left(-i \int_0^t \mathcal{H}_{\alpha\beta}(t') dt'\right) |\nu_\beta\rangle_0, \quad (2)$$

where $|\nu_\beta\rangle_0$ corresponds to the initial flavor state. In vacuum, the Hamiltonian describing the neutrino evolution is $\mathcal{H}(t) = U\mathcal{M}^2U^*/E(t)$. Here U stands for the lepton mixing matrix, which relates the mass and flavor eigenstates, $|\nu_\alpha\rangle = U_{\alpha i}^* |\nu_i\rangle$, and $\mathcal{M}^2 = \text{diag}(m_1^2, \dots)$ is the diagonal mass-squared matrix.

In the case of extra-galactic sources, the expansion of the universe modifies the phase of the flavor state as neutrinos propagate, having an impact on the final flavor distribution if the oscillations are not averaged out. In the case of a homogeneous and isotropic universe, the expansion is encoded in the scale factor ($a(t)$) that depends on the redshift (z) as $1+z = a_0/a$, a_0 being the scale factor today ($a_0 = 1$ for a flat universe). The expansion rate of the universe is given by the Hubble parameter $H = \dot{a}/a$, where $\dot{a} \equiv da/dt$. As the universe expands, there is a redshift in the neutrino energy that will also affect the phase of the flavor states. The relation between the initial (E'_ν) and the redshifted (E_ν) neutrino energies is $E_\nu = E'_\nu/(1+z)$. The time-integration of the Hamiltonian is given by

$$\int \mathcal{H}(t) dt = \frac{U\mathcal{M}^2U^*}{E_\nu} \int \frac{dz}{H(z)(1+z)^2} \equiv \frac{U\mathcal{M}^2U^*}{E_\nu} L_{\text{eff}}. \quad (3)$$

The relation between the Hubble parameter and the redshift is given by

$$H(z) = H_0 \sqrt{\Omega_m(1+z)^3 + \Omega_\Lambda + (1 - \Omega_m - \Omega_\Lambda)(1+z)^2}, \quad (4)$$

where Ω_m and Ω_Λ are the fractions of matter and dark energy content, and H_0 is the present value of the Hubble constant. For those parameters, we used the best-fit value from Planck [43] results. On astrophysical scales, the phase the flavor states get depends on the universe's expansion via the effective distance (L_{eff}).

In the pseudo-Dirac scenario, the mixing between the flavor and the mass eigenstates is $\nu_\alpha = U_{\alpha i}(\nu_{iS} + \nu_{iA})/\sqrt{2}$, where $U_{\alpha i}$ is the PMNS matrix. Considering redshift dependence in the neutrino evolution, the probability that a flavor state ν_α oscillates into a flavor state ν_β is given by

$$P_{\alpha\beta} = \frac{1}{4} \left| \sum_{j=1}^3 U_{\beta j} U_{\alpha j}^* \left\{ e\left(\frac{im_{jS}^2 L_{\text{eff}}}{2E_\nu}\right) + e\left(\frac{im_{jA}^2 L_{\text{eff}}}{2E_\nu}\right) \right\} \right|^2 \quad (5)$$

where m_{jA}^2 and m_{jS}^2 are the masses of the symmetric and anti-symmetric combinations of the active and sterile states, respectively. The oscillation probability has two well-separated oscillation lengths: For $\Delta m_{ij}^2 =$

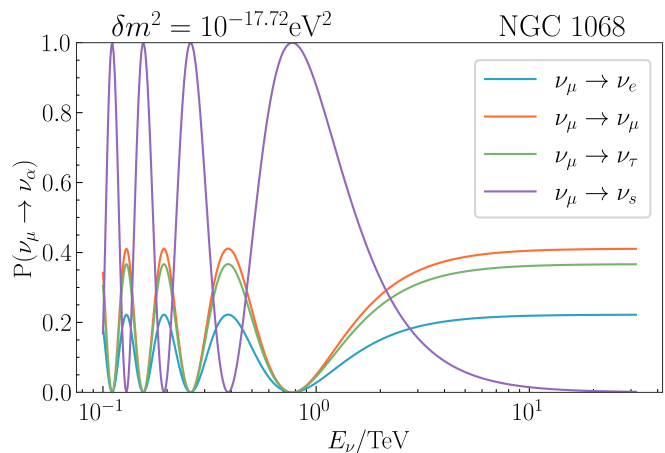


FIG. 2. Oscillation probability of ν_μ into active and sterile components as a function of the neutrino energy for a benchmark value of $\delta m^2 = 10^{-17.72} \text{eV}^2$ for all three active-sterile pairs, and for the redshift of NGC 1068 ($z = 0.0038$).

$m_{iS/A}^2 - m_{jS/A}^2 \sim 10^{-3} \text{eV}^2$ (atmospheric mass splitting) or $\sim 10^{-5} \text{eV}^2$ (solar mass splitting), the oscillation length is of the order of $L_{\text{osc}} = 4\pi E/\Delta m_{ij}^2 \sim 10^7 - 10^9 \text{km}$ for $E_\nu \sim 10 \text{TeV}$, which is comparable to the Earth-Sun distance. But for the active-sterile mass splitting (δm^2), the oscillation length will be much larger, depending on the magnitude of M_R . Taking the average over the large mass splittings, the oscillation probability becomes

$$P_{\alpha\beta} = \frac{1}{2} \sum_{j=1}^3 |U_{\beta j}|^2 |U_{\alpha j}|^2 \left[1 + \cos\left(\frac{\delta m_j^2 L_{\text{eff}}}{2E_\nu}\right) \right]. \quad (6)$$

Thus, the oscillation probability depends only on the three mass splittings, one for each pair of degenerate masses.³ For illustration, in Figure 2 we show the probability of muon neutrinos oscillating into active and sterile neutrinos for all the three mass splittings equal to $\delta m^2 = 10^{-17.72} \text{eV}^2$ and redshift $z = 0.0038$, corresponding to NGC 1068. With regard to the lepton-mixing matrix, we used the best-fit from [44]. For this mass splitting, and $E_\nu \sim \text{TeV}$, all the muon neutrinos arrive to the Earth as sterile states.

Analysis.— The discovery of high-energy extra-galactic neutrinos by the IceCube Neutrino Observatory [45, 46] marked the beginning of a new era of neutrino astronomy. According to the latest results [1], the three astrophysical sources identified with the most significance are the active galactic nuclei NGC 1068, PKS 1424+240, and TXS 0506+056, with local significance of 5.2σ , 3.7σ , and 3.5σ respectively. IceCube's

³ In the case where the mass difference is the same for the three pairs, all the flavors will oscillate with the same frequency.

point-source search used only track-like events, which have an excellent angular resolution [47, 48] ($\Delta\delta < 1^\circ$). In addition, they assumed that the neutrino flux followed a power-law and found that the event distribution of each source was best described by spectral indices $\hat{\gamma} = 3.2, 3.5$, and 2.0, and total event counts $\hat{n}_s = 79, 77$, and 5, respectively; see Table I. These sources are located at different redshifts $z = 0.0038$ [49], 0.6047 [50], and 0.3367 [51], corresponding to approximately 16 Mpc, 2.6 Gpc and 1.4 Gpc, respectively.

We calculate the expected number of IceCube track-like events from each source under the standard and pseudo-Dirac hypotheses. To predict the expected number of events, we use the effective area given in Ref. [47]. We assume that the neutrino production mechanism is charged pion decay, so the flavor composition is equal to (1:2:0) at the source. As a benchmark scenario, we consider an initial neutrino flux following an unbroken power-law distribution in energy from 100 GeV onwards, with spectral indices given by the best-fit values from Ref. [1], see Table I. We compute the expected number of events in a reconstructed energy bin by integrating the flux and effective area over true energy, weighted by the reconstruction probability. IceCube’s energy resolution for through-going muons is about 30% in log-energy scale, so we model this probability distribution as a Gaussian with width 0.30 [52]. We explore the effect of varying the energy resolution in Appendix B. All the numerical calculations were done in Julia [53].

The expected event distributions for NGC 1068, PKS 1424+240, and TXS 0506+056 for a lifetime of 3168 days are shown in Figure 3. The pseudo-Dirac expectations, plotted in color, predict fewer events than the SM (black curve), since neutrinos that oscillate from active to sterile become undetectable. Since each source has a different initial flux and a different redshift value, each is sensitive to different regions of the pseudo-Dirac parameter space.

We then calculate IceCube’s sensitivity to a pseudo-Dirac signal by performing a likelihood ratio test. For each value of an active-sterile mass splitting, held equal over all three mass states, we calculate the Poisson likelihood of observing the SM prediction under a pseudo-Dirac hypothesis. This procedure results in an optimistic sensitivity, since it does not account for the uncertainty in the background removal. A slightly more conservative result could be achieved by using an effective likelihood with modeling uncertainty [54]. We treat the flux normalization and spectral index as nuisance parameters. For numerical optimization, we used the package `Optim` [55] in Julia.

Our results focus on the scenario where the three mass splittings are equal. This subset of the pseudo-Dirac parameter space contains the points to which we are most sensitive, because all the mass states contribute to the active-sterile oscillation at the same energies. Sensitivity

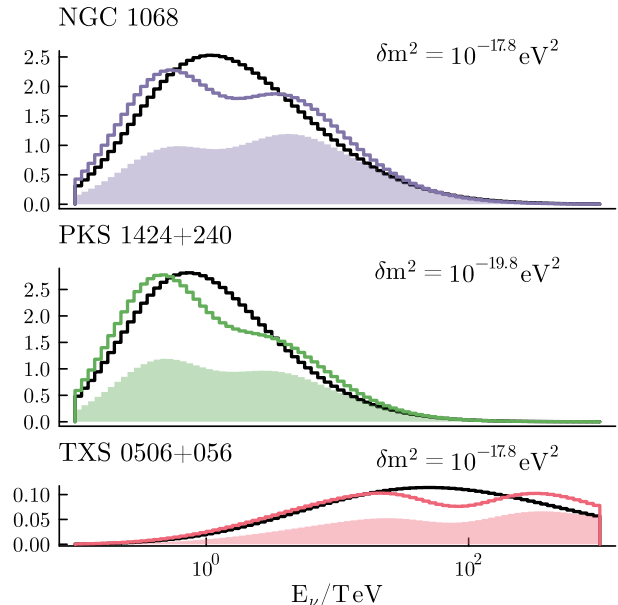


FIG. 3. Calculated event distributions for the three most significant sources under the SM (black) and the pseudo-Dirac (filled color) hypotheses. The latter are plotted considering uniform sterile-active mass splittings for all three pairs of mass states; the value used in each source’s calculation is printed in the upper right corner. When we maximize the likelihood that the pseudo-Dirac hypothesis can describe SM-like data, by allowing the flux parameters to vary, (color) the difference between the two distributions is reduced.

to the scenario where two mass splittings differ from zero independently is explored in Appendix C.

Results.— In this *Letter*, we perform a combined analysis of the expected event distribution of the three most significant astrophysical sources (NGC 1068, PKS 1424+240, and TXS 0506+056) observed by IceCube. Because the sources are unequally distant from the Earth and have different spectral indices, they are each sensitive to different regions of the δm^2 parameter space. Combining them, we explore for the first time mass-splittings in the range $\delta m^2 \in [10^{-21}, 10^{-16}]eV^2$.

The results of the sensitivity analysis are shown in Figure 4. For TeV sources, the redshift of each source fixes the effective distance, L_{eff} , and thus the scale of the mass-splittings to which it is sensitive. The spectral index of each source sets the distribution of its events over energy, which controls the width of the range of mass-splittings to which it is sensitive. Thus NGC 1068 and PKS 1424+240, which both have relatively soft spectra but have redshifts three orders apart, are sensitive to two very different, concentrated regions of parameter space. Conversely, TXS 0506+056, which has a much softer spectra, is sensitive to a wide region, although its sensitivity is limited by its small best-fit event count (5

events).

At small values of the mass splitting ($\delta m^2 \sim 10^{-21} \text{eV}^2$), the sensitivity is dominated by PKS 1424+240, reaching $\sim 5\sigma$ for $\delta m^2 \sim 10^{-20} \text{eV}^2$. Interestingly, mass splittings on the same order have previously been explored using data from supernova SN1987A [13] (vertical grey-shaded region). For masses around $\delta m^2 \sim 10^{-18} \text{eV}^2$, the sensitivity is dominated by NGC 1068. The vertical line to the left of the plot indicates the left-edge of the region motivated by a $B - L$ gauge symmetry.

In supplemental analyses, we also consider whether a pseudo-Dirac signal would be recoverable. In Appendix D we calculate the likelihood of SM and pseudo-Dirac hypotheses, given data following a pseudo-Dirac prediction for two possible values of the equal mass-splitting. We find that the maximum-likelihood point corresponds to the true value. A pseudo-Dirac reality would also impact studies of source fluxes, by shifting the inferred spectral index with respect to the true value. We explore this possibility in in Appendix E, and find the effect could be as large as an 8% shift. This effect could also impact diffuse neutrino fluxes, since distortions to the source flux caused by pseudo-Dirac disappearances could accumulate. Finally, in Appendix F we explore the possibility of improving IceCube’s current sensitivity by separating events into tracks which start within the detector volume, which have superior energy resolution, and those which traverse it. This possibility was not included in the main analysis because the starting event fraction is not publicly available.

In the lower part of Figure 4, we show the projected sensitivity of IceCube-Gen2. For this analysis, we included all the sources which IceCube can currently identify with at least 1.1σ local significance, and for which there exists a published redshift value; see Table I. Additionally, we multiply all statistics by a factor of 8, as projected by Ref. [56]. We find that the combined sensitivity is well past 3σ over a wide range of mass splittings.

Conclusions.—

In this *Letter*, we investigated IceCube’s current and future sensitivity to the pseudo-Dirac neutrino mass scenario. The combined analysis of the three most significant astrophysical sources observed by IceCube probes active-sterile mass-splittings in the range $10^{-20} \text{eV}^2 < \delta m^2 < 10^{-16} \text{eV}^2$, but its sensitivity is limited by statistics and poor energy resolution. However, by including sources observed by IceCube with a significance larger than 1.1σ , and assuming 8 times greater statistics, we found that IceCube-Gen2 will be able to explore a large range of masses with a significance over 5σ .

Next-generation neutrino telescopes [57–64] will unveil a constellation of neutrino sources, opening the possibility of exploring very long baseline neutrino physics. By combining many astrophysical sources, over a wide range of distances, we will gain access to a broad and hitherto

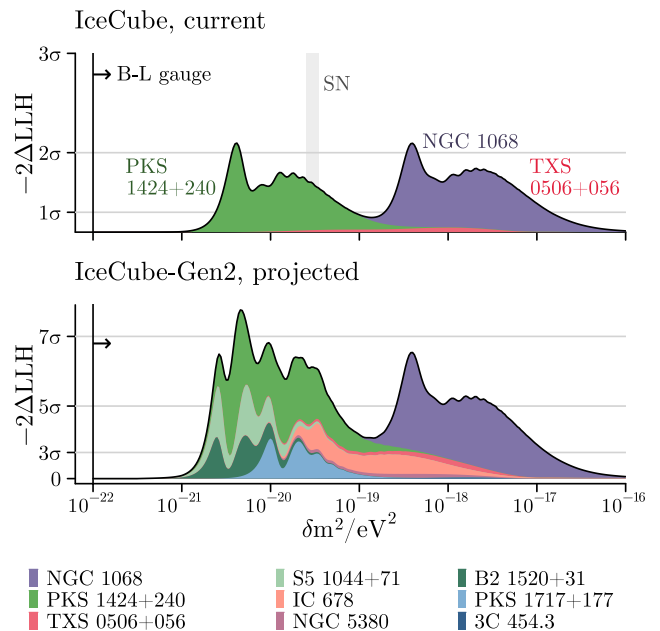


FIG. 4. *Top*: The log-likelihood ratio ΔLLH of the combined analysis with the three currently significant sources (black) overlaid with that of each separately (color). The gray-shaded region indicates the 3σ region excluded by SN 1987 A. *Bottom*: Projected sensitivity of IceCube Gen2, using nine astrophysical sources and assuming 8x statistics. Sensitivity from each source is stacked; the total is shown by the black curve.

unexplored range of active-sterile mass splittings. The expected signal, a dip in the neutrino spectra, due to the oscillation into the sterile state, must be observed in all the sources sharing a common L_{eff}/E . This signature is robust under uncertainties in astrophysical neutrino fluxes, which at this early point are significant.

The pseudo-Dirac hypothesis can also modify the flavor ratio of high-energy neutrinos at IceCube. In presence of active-sterile oscillations, the flavor composition on Earth is expected to be different from the conventional (1:1:1) for a (1:2:0) source composition [65], depending on the flavor structure of the neutrino mass matrix (1). Unfortunately, reconstructing the flavor triangle in this case will require both cascade and track events from the identified sources. The poor angular resolution of the cascades ($\Delta\delta \sim 1^\circ$, as compared to $\Delta\delta \lesssim 0.1^\circ$ for tracks) makes this task rather difficult, but it may be possible with future neutrino telescopes.

This *Letter* strongly motivates a full likelihood-based analysis by the IceCube collaboration. A more descriptive flux hypothesis would alter the significance of the source identification and the maximum likelihood parameters. This full likelihood analysis should be unbinned, consider background and signal simultaneously, and include a full treatment of detector systematics. Only such a study would be able to unambiguously resolve

the pseudo-Dirac nature of neutrinos.

Acknowledgments — We thank Matthew Reece and William Thompson for useful comments. We also thank Jack Pairin for his artwork. CAA and IMS are supported by the Faculty of Arts and Sciences of Harvard University and the Alfred P. Sloan Foundation. KC is supported by the NSF Graduate Research Fellowship under Grant No. 2140743. KSB is supported in part by the US Department of Energy grant No. DE-SC 0016013. BD is supported by the US Department of Energy grant No. DE-SC 0017987 and by a URA VSP fellowship. We thank the organizers of the NTN workshop at Fermilab in June 2022 for local hospitality where this work was initiated.

* kcarloni@g.harvard.edu

† imartinezsoler@fas.harvard.edu

‡ carguelles@fas.harvard.edu

§ kaladi.babu@okstate.edu

¶ bdev@wustl.edu

- [1] R. Abbasi *et al.* (IceCube), Evidence for neutrino emission from the nearby active galaxy NGC 1068, *Science* **378**, 538 (2022).
- [2] K. Wright, Neutrino Astronomy Enters a New Era, *APS Physics* **15**, 171 (2022).
- [3] L. Wolfenstein, Different Varieties of Massive Dirac Neutrinos, *Nucl. Phys. B* **186**, 147 (1981).
- [4] S. T. Petcov, On Pseudodirac Neutrinos, Neutrino Oscillations and Neutrinoless Double beta Decay, *Phys. Lett. B* **110**, 245 (1982).
- [5] J. W. F. Valle and M. Singer, Lepton Number Violation With Quasi Dirac Neutrinos, *Phys. Rev. D* **28**, 540 (1983).
- [6] M. Kobayashi and C. S. Lim, Pseudo Dirac scenario for neutrino oscillations, *Phys. Rev. D* **64**, 013003 (2001), [arXiv:hep-ph/0012266](#).
- [7] J. F. Beacom, N. F. Bell, D. Hooper, J. G. Learned, S. Pakvasa, and T. J. Weiler, PseudoDirac neutrinos: A Challenge for neutrino telescopes, *Phys. Rev. Lett.* **92**, 011101 (2004), [arXiv:hep-ph/0307151](#).
- [8] P. Keranen, J. Maalampi, M. Myrskylainen, and J. Riittinen, Effects of sterile neutrinos on the ultrahigh-energy cosmic neutrino flux, *Phys. Lett. B* **574**, 162 (2003), [arXiv:hep-ph/0307041](#).
- [9] A. Esmaili, Pseudo-Dirac Neutrino Scenario: Cosmic Neutrinos at Neutrino Telescopes, *Phys. Rev. D* **81**, 013006 (2010), [arXiv:0909.5410 \[hep-ph\]](#).
- [10] A. Esmaili and Y. Farzan, Implications of the Pseudo-Dirac Scenario for Ultra High Energy Neutrinos from GRBs, *JCAP* **12**, 014, [arXiv:1208.6012 \[hep-ph\]](#).
- [11] V. Brdar and R. S. L. Hansen, IceCube Flavor Ratios with Identified Astrophysical Sources: Towards Improving New Physics Testability, *JCAP* **02**, 023, [arXiv:1812.05541 \[hep-ph\]](#).
- [12] A. De Gouvêa, I. Martinez-Soler, Y. F. Perez-Gonzalez, and M. Sen, Fundamental physics with the diffuse supernova background neutrinos, *Phys. Rev. D* **102**, 123012 (2020), [arXiv:2007.13748 \[hep-ph\]](#).
- [13] I. Martinez-Soler, Y. F. Perez-Gonzalez, and M. Sen, Signs of pseudo-Dirac neutrinos in SN1987A data, *Phys. Rev. D* **105**, 095019 (2022), [arXiv:2105.12736 \[hep-ph\]](#).
- [14] P. Minkowski, $\mu \rightarrow e\gamma$ at a Rate of One Out of 10^9 Muon Decays?, *Phys. Lett. B* **67**, 421 (1977).
- [15] R. N. Mohapatra and G. Senjanovic, Neutrino Mass and Spontaneous Parity Nonconservation, *Phys. Rev. Lett.* **44**, 912 (1980).
- [16] T. Yanagida, Horizontal gauge symmetry and masses of neutrinos, *Conf. Proc. C* **7902131**, 95 (1979).
- [17] M. Gell-Mann, P. Ramond, and R. Slansky, Complex Spinors and Unified Theories, *Conf. Proc. C* **790927**, 315 (1979), [arXiv:1306.4669 \[hep-th\]](#).
- [18] Z. K. Silagadze, Neutrino mass and the mirror universe, *Phys. Atom. Nucl.* **60**, 272 (1997), [arXiv:hep-ph/9503481](#).
- [19] A. S. Josphipura, S. Mohanty, and S. Pakvasa, Pseudo-Dirac neutrinos via a mirror world and depletion of ultra-high energy neutrinos, *Phys. Rev. D* **89**, 033003 (2014), [arXiv:1307.5712 \[hep-ph\]](#).
- [20] P.-H. Gu and H.-J. He, Neutrino Mass and Baryon Asymmetry from Dirac Seesaw, *JCAP* **12**, 010, [arXiv:hep-ph/0610275](#).
- [21] E. Ma and R. Srivastava, Dirac or inverse seesaw neutrino masses with $B - L$ gauge symmetry and S_3 flavor symmetry, *Phys. Lett. B* **741**, 217 (2015), [arXiv:1411.5042 \[hep-ph\]](#).
- [22] J. W. F. Valle and C. A. Vaquera-Araujo, Dynamical seesaw mechanism for Dirac neutrinos, *Phys. Lett. B* **755**, 363 (2016), [arXiv:1601.05237 \[hep-ph\]](#).
- [23] S. Centelles Chuliá, R. Srivastava, and J. W. F. Valle, Seesaw Dirac neutrino mass through dimension-six operators, *Phys. Rev. D* **98**, 035009 (2018), [arXiv:1804.03181 \[hep-ph\]](#).
- [24] T. D. Lee and C.-N. Yang, Question of Parity Conservation in Weak Interactions, *Phys. Rev.* **104**, 254 (1956).
- [25] R. Foot, H. Lew, and R. R. Volkas, Possible consequences of parity conservation, *Mod. Phys. Lett. A* **7**, 2567 (1992).
- [26] Z. G. Berezhiani and R. N. Mohapatra, Reconciling present neutrino puzzles: Sterile neutrinos as mirror neutrinos, *Phys. Rev. D* **52**, 6607 (1995), [arXiv:hep-ph/9505385](#).
- [27] S. Weinberg, Baryon and Lepton Nonconserving Processes, *Phys. Rev. Lett.* **43**, 1566 (1979).
- [28] A. de Gouvea, W.-C. Huang, and J. Jenkins, Pseudo-Dirac Neutrinos in the New Standard Model, *Phys. Rev. D* **80**, 073007 (2009), [arXiv:0906.1611 \[hep-ph\]](#).
- [29] S. Ansarifard and Y. Farzan, Revisiting pseudo-Dirac neutrino scenario after recent solar neutrino data, (2022), [arXiv:2211.09105 \[hep-ph\]](#).
- [30] R. Barbieri and A. Dolgov, Bounds on Sterile-neutrinos from Nucleosynthesis, *Phys. Lett. B* **237**, 440 (1990).
- [31] K. Enqvist, K. Kainulainen, and J. Maalampi, Resonant neutrino transitions and nucleosynthesis, *Phys. Lett. B* **249**, 531 (1990).
- [32] G. Aad *et al.* (ATLAS), Search for high-mass dilepton resonances using 139 fb^{-1} of pp collision data collected at $\sqrt{s} = 13 \text{ TeV}$ with the ATLAS detector, *Phys. Lett. B* **796**, 68 (2019), [arXiv:1903.06248 \[hep-ex\]](#).
- [33] *Search for a narrow resonance in high-mass dilepton final states in proton-proton collisions using 140 fb^{-1} of data at $\sqrt{s} = 13 \text{ TeV}$* , Tech. Rep. (2019) cMS-PAS-EXO-19-019.
- [34] R. N. Mohapatra, A Model for Dirac Neutrino Masses

- and Mixings, *Phys. Lett. B* **198**, 69 (1987).
- [35] K. S. Babu and X. G. He, Dirac neutrino masses as two-loop radiative corrections, *Mod. Phys. Lett. A* **4**, 61 (1989).
- [36] Y. Farzan and E. Ma, Dirac neutrino mass generation from dark matter, *Phys. Rev. D* **86**, 033007 (2012), [arXiv:1204.4890 \[hep-ph\]](#).
- [37] E. Ma and O. Popov, Pathways to Naturally Small Dirac Neutrino Masses, *Phys. Lett. B* **764**, 142 (2017), [arXiv:1609.02538 \[hep-ph\]](#).
- [38] S. Saad, Simplest Radiative Dirac Neutrino Mass Models, *Nucl. Phys. B* **943**, 114636 (2019), [arXiv:1902.07259 \[hep-ph\]](#).
- [39] S. Jana, P. K. Vishnu, and S. Saad, Minimal dirac neutrino mass models from $U(1)_R$ gauge symmetry and left–right asymmetry at colliders, *Eur. Phys. J. C* **79**, 916 (2019), [arXiv:1904.07407 \[hep-ph\]](#).
- [40] K. S. Babu, X.-G. He, M. Su, and A. Thapa, Naturally light Dirac and pseudo-Dirac neutrinos from left-right symmetry, *JHEP* **08**, 140, [arXiv:2205.09127 \[hep-ph\]](#).
- [41] K. S. Babu, P. S. B. Dev, S. Jana, and Y. Sui, Zee-Burst: A New Probe of Neutrino Nonstandard Interactions at IceCube, *Phys. Rev. Lett.* **124**, 041805 (2020), [arXiv:1908.02779 \[hep-ph\]](#).
- [42] K. S. Babu, P. S. B. Dev, and S. Jana, Probing neutrino mass models through resonances at neutrino telescopes, *Int. J. Mod. Phys. A* **37**, 2230003 (2022), [arXiv:2202.06975 \[hep-ph\]](#).
- [43] N. Aghanim *et al.* (Planck), Planck 2018 results. VI. Cosmological parameters, *Astron. Astrophys.* **641**, A6 (2020), [Erratum: *Astron. Astrophys.* 652, C4 (2021)], [arXiv:1807.06209 \[astro-ph.CO\]](#).
- [44] I. Esteban, M. C. Gonzalez-Garcia, M. Maltoni, T. Schwetz, and A. Zhou, The fate of hints: updated global analysis of three-flavor neutrino oscillations, *JHEP* **09**, 178, [arXiv:2007.14792 \[hep-ph\]](#).
- [45] M. G. Aartsen *et al.* (IceCube), First observation of PeV-energy neutrinos with IceCube, *Phys. Rev. Lett.* **111**, 021103 (2013), [arXiv:1304.5356 \[astro-ph.HE\]](#).
- [46] M. G. Aartsen *et al.* (IceCube), Evidence for High-Energy Extraterrestrial Neutrinos at the IceCube Detector, *Science* **342**, 1242856 (2013), [arXiv:1311.5238 \[astro-ph.HE\]](#).
- [47] M. G. Aartsen *et al.* (IceCube), All-sky Search for Time-integrated Neutrino Emission from Astrophysical Sources with 7 yr of IceCube Data, *Astrophys. J.* **835**, 151 (2017), [arXiv:1609.04981 \[astro-ph.HE\]](#).
- [48] R. Abbasi *et al.* (IceCube), IceCube Data for Neutrino Point-Source Searches Years 2008-2018 [10.21234/CPKQ-K003](#) (2021), [arXiv:2101.09836 \[astro-ph.HE\]](#).
- [49] M. J. Meyer *et al.*, The HIPASS Catalog. I. Data presentation, *Mon. Not. Roy. Astron. Soc.* **350**, 1195 (2004), [arXiv:astro-ph/0406384](#).
- [50] S. Paiano, M. Landoni, R. Falomo, A. Treves, R. Scarpa, and C. Righi, On the Redshift of TeV BL Lac Objects, *Astrophys. J.* **837**, 144 (2017), [arXiv:1701.04305 \[astro-ph.GA\]](#).
- [51] S. Paiano, R. Falomo, A. Treves, and R. Scarpa, The redshift of the BL Lac object TXS 0506+056, *Astrophys. J. Lett.* **854**, L32 (2018), [arXiv:1802.01939 \[astro-ph.GA\]](#).
- [52] M. G. Aartsen *et al.* (IceCube), Energy Reconstruction Methods in the IceCube Neutrino Telescope, *JINST* **9**, P03009, [arXiv:1311.4767 \[physics.ins-det\]](#).
- [53] J. Bezanson, A. Edelman, S. Karpinski, and V. B. Shah, Julia: A fresh approach to numerical computing, *SIAM review* **59**, 65 (2017).
- [54] C. A. Argüelles, A. Schneider, and T. Yuan, A binned likelihood for stochastic models, *JHEP* **06**, 030, [arXiv:1901.04645 \[physics.data-an\]](#).
- [55] P. K. Mogensen and A. N. Riseth, Optim: A mathematical optimization package for Julia, *Journal of Open Source Software* **3**, 615 (2018).
- [56] N. Song, S. W. Li, C. A. Argüelles, M. Bustamante, and A. C. Vincent, The Future of High-Energy Astrophysical Neutrino Flavor Measurements, *JCAP* **04**, 054, [arXiv:2012.12893 \[hep-ph\]](#).
- [57] M. G. Aartsen *et al.* (IceCube-Gen2), IceCube-Gen2: the window to the extreme Universe, *J. Phys. G* **48**, 060501 (2021), [arXiv:2008.04323 \[astro-ph.HE\]](#).
- [58] S. Adrian-Martinez *et al.* (KM3Net), Letter of intent for KM3NeT 2.0, *J. Phys. G* **43**, 084001 (2016), [arXiv:1601.07459 \[astro-ph.IM\]](#).
- [59] M. Agostini *et al.* (P-ONE), The Pacific Ocean Neutrino Experiment, *Nature Astron.* **4**, 913 (2020), [arXiv:2005.09493 \[astro-ph.HE\]](#).
- [60] J. Álvarez-Muñiz *et al.* (GRAND), The Giant Radio Array for Neutrino Detection (GRAND): Science and Design, *Sci. China Phys. Mech. Astron.* **63**, 219501 (2020), [arXiv:1810.09994 \[astro-ph.HE\]](#).
- [61] A. Neronov, D. V. Semikoz, L. A. Anchordoqui, J. Adams, and A. V. Olinto, Sensitivity of a proposed space-based Cherenkov astrophysical-neutrino telescope, *Phys. Rev. D* **95**, 023004 (2017), [arXiv:1606.03629 \[astro-ph.IM\]](#).
- [62] M. Sasaki and T. Kifune, Ashra Neutrino Telescope Array (NTA): Combined Imaging Observation of Astroparticles — For Clear Identification of Cosmic Accelerators and Fundamental Physics Using Cosmic Beams —, *JPS Conf. Proc.* **15**, 011013 (2017).
- [63] A. Romero-Wolf *et al.*, An Andean Deep-Valley Detector for High-Energy Tau Neutrinos, in *Latin American Strategy Forum for Research Infrastructure* (2020) [arXiv:2002.06475 \[astro-ph.IM\]](#).
- [64] A. V. Olinto *et al.* (POEMMA), The POEMMA (Probe of Extreme Multi-Messenger Astrophysics) observatory, *JCAP* **06**, 007, [arXiv:2012.07945 \[astro-ph.IM\]](#).
- [65] J. G. Learned and S. Pakvasa, Detecting tau-neutrino oscillations at PeV energies, *Astropart. Phys.* **3**, 267 (1995), [arXiv:hep-ph/9405296 \[hep-ph\]](#).
- [66] A. G. Polatidis, P. N. Wilkinson, W. Xu, A. C. S. Readhead, T. J. Pearson, G. B. Taylor, and R. C. Vermeulen, The First Caltech–Jodrell Bank VLBI Survey. I. $\lambda = 18$ Centimeter Observations of 87 Sources, *??jnlApJS* **98**, 1 (1995).
- [67] F. D. Albareti *et al.* (SDSS), The 13th Data Release of the Sloan Digital Sky Survey: First Spectroscopic Data from the SDSS-IV Survey Mapping Nearby Galaxies at Apache Point Observatory, *Astrophys. J. Suppl.* **233**, 25 (2017), [arXiv:1608.02013 \[astro-ph.GA\]](#).
- [68] J. P. Huchra, M. J. Geller, and J. Corwin, Harold G., The cfa redshift survey: Data for the ngp +36 zone, *The Astrophysical Journal Supplement Series* **99**, 391 (1995).
- [69] D. Sowards-Emmerd, R. W. Romani, P. F. Michelson, S. E. Healey, and P. L. Nolan, A northern survey of gamma-ray blazar candidates, *The Astrophysical Journal* **626**, 95 (2005).
- [70] M. T. Murphy, G. G. Kacprzak, G. A. D. Sa-

vorgnan, and R. F. Carswell, The UVES Spectral Quasar Absorption Database (SQUAD) data release 1: the first 10 million seconds, *Monthly Notices of the Royal Astronomical Society* **482**, 3458 (2018), <https://academic.oup.com/mnras/article-pdf/482/3/3458/26677231/sty2834.pdf>.

- [71] A. Palladino and W. Winter, A multi-component model for observed astrophysical neutrinos, *Astronomy & Astrophysics* **615**, A168 (2018).
- [72] A. Garcia Soto, New sensitivities for ev-scale sterile neutrino searches with icecube (2022).

Supplemental Material

Appendix A: Candidate astrophysical sources

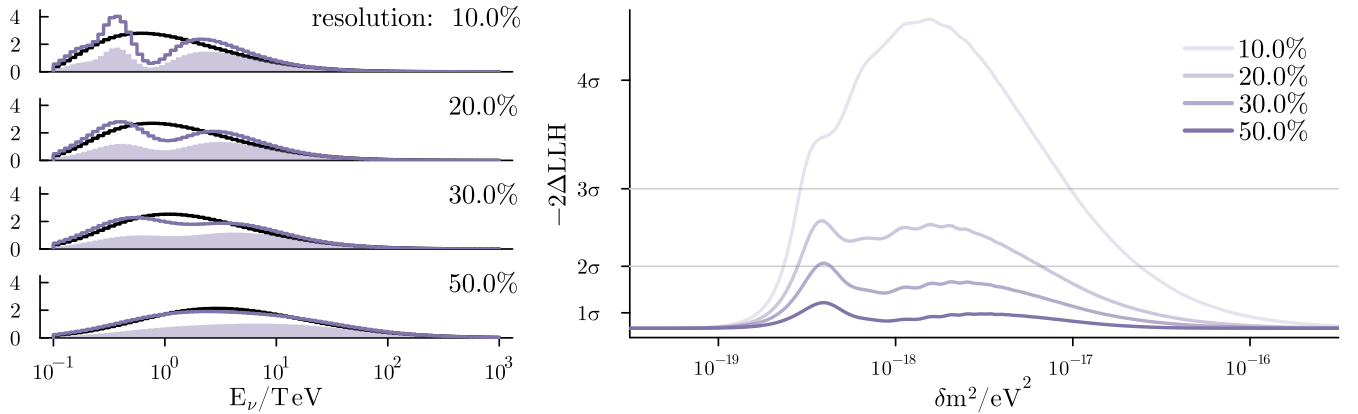
Source	Source Type	$-\log_{10} p_{\text{local}}$	\hat{n}_s	$\hat{\gamma}$	z	z Ref.
NGC 1068	SBG/AGN	7.0	79	3.2	0.0038 ± 0.00001	[49]
PKS 1424+240	BLL	4.0	77	3.5	0.6047 ± 0.1	[50]
TXS 0506+056	BLL/FSRQ	3.6	5	2.0	0.3365 ± 0.001	[51]
S5 1044+71	FSRQ	1.3	45	4.3	1.1500	[66]
IC 678	GAL	0.9	22	3.1	0.04799 ± 0.00002	[67]
NGC 5380	GAL	0.9	4	2.4	0.010584 ± 0.000077	[68]
B2 1520+31	FSRQ	1.0	35	4.3	1.48875 ± 0.00025	[67]
PKS 1717+177	BLL	1.0	34	4.3	0.137	[69]
3C 454.3	FSRQ	1.2	1	1.5	0.859	[70]

SUPPL. TABLE I. The nine astrophysical sources considered in this work. The first three are the most significant. The maximum likelihood values $-\log_{10} p_{\text{local}}, \hat{n}_s, \hat{\gamma}$ are copied from Ref. [1]. The redshifts are obtained from different sources, as listed in the last column. The source GB6 J1542+6129, which was identified by Ref. [1] with local significance of 2.2σ , was not included in this analysis, as its redshift is poorly constrained.

Appendix B: Energy resolution and sensitivity

The energy resolution of the IceCube detector significantly affects the ability to resolve a dip in the event distribution. In this section we demonstrate this effect. We model the probability of an event with given reconstructed log-energy having a particular true value as a Gaussian with variable width. On the left side of Figure B.1, we plot the event distributions at $\delta m^2 = 10^{-17.8} \text{eV}^2$ for different values of this energy resolution, while on the right side we plot the corresponding sensitivity to the pseudo-Dirac parameter space. As the resolution improves, the pseudo-Dirac disappearance effect increases in clarity, and the sensitivity leaps upward.

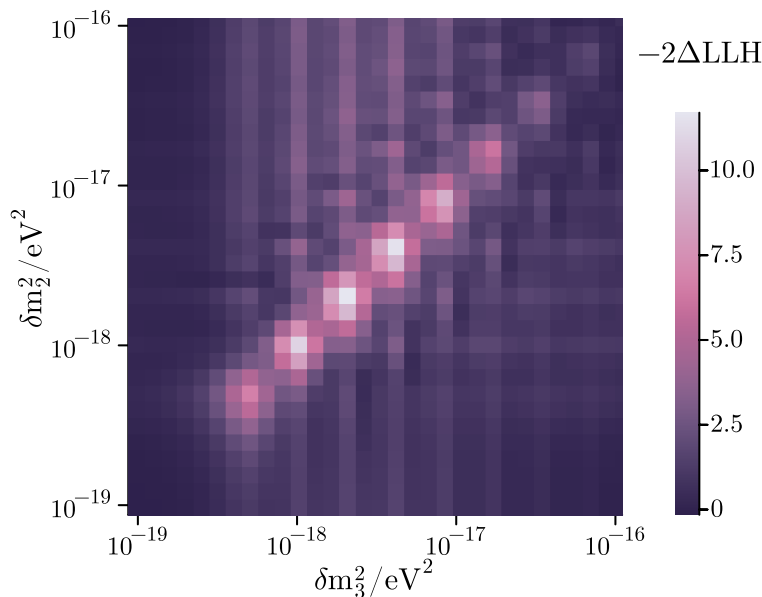
The Gaussian model used here is only an approximation to the reconstructed energy distribution. Generally, the true energy of an event can be significantly underestimated by reconstruction algorithms when the track length extends far beyond the detector confines. This underestimation effect results in a true energy probability distribution with a long asymmetric tail. Additionally, this effect is enhanced for higher-energy events, which travel much further in the ice.



SUPPL. FIG. B.1. Event distributions (*left*) and sensitivities (*right*) for different values of the log-energy resolution, using NGC 1068 as the source.

Appendix C: Sensitivity to distinct mass splittings

Although most of this analysis focused on the subset of parameter space in which all three pseudo-Dirac mass splittings are equal, we have also performed a scan for the sensitivity to distinct mass splittings. Because this work focuses on track-like events in IceCube, whose direction can be reconstructed to sub-degree precision, the mass splittings $\delta m_2^2, \delta m_3^2$ are much more significant than δm_1^2 . This is due to the fact that track-like events are predominantly produced by muon neutrinos, and the mass states ν_2, ν_3 are more likely to be measured in the flavor basis as ν_μ than ν_1 .



SUPPL. FIG. C.1. Sensitivity to the pseudo-Dirac parameter space with distinct mass splittings. Here we have varied δm_2^2 and δm_3^2 , with fixed $\delta m_1^2 = 0.0$.

In Figure C.1 we plot the test statistic $-2\Delta\text{LLH}$, corresponding to the likelihood ratio of the pseudo-Dirac hypothesis to the SM, calculated for data simulated according to the SM prediction for NGC 1068. In this section we also assume near-perfect energy reconstruction. The sensitivity is maximized at the center of the diagonal, where a maximum number of neutrinos in both mass states ν_2, ν_3 are oscillating into their sterile counterparts and disappearing.

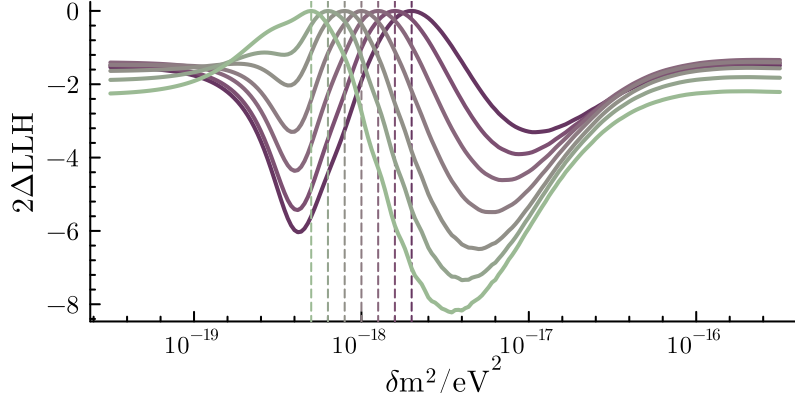
Appendix D: Injection and recovery of true pseudo-Dirac parameters

In this section, we consider whether a maximum likelihood fit would be able to recover the true pseudo-Dirac parameter values. Using the event distribution of the source NGC 1068, we generate an event distribution according to an injected uniform pseudo-Dirac mass splitting, δm_{true}^2 and then calculate the likelihood of this distribution under a different pseudo-Dirac hypothesis, δm^2 . The test statistic $2\Delta\text{LLH}$ is plotted for a spectrum of injected δm_{true}^2 in Figure D.1.

In all cases the likelihood difference is maximized at the injected value. The likelihood of the SM hypothesis can be equated with the limit $\delta m^2 = 0$ in this plot, i.e. the limiting value of the left-hand side.

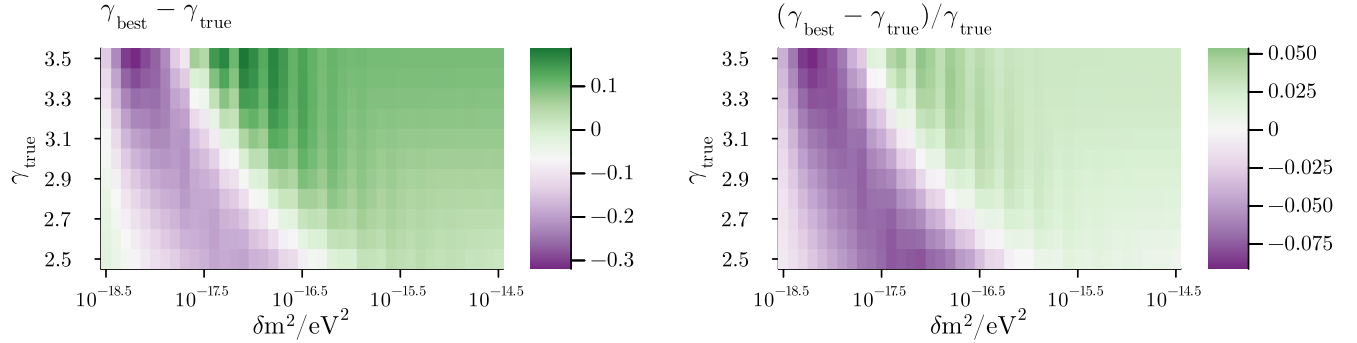
Appendix E: Standard Model fits to pseudo-Dirac reality

We also consider how a maximum likelihood fit for source flux parameters (normalization and spectral index) which assumed a Standard Model hypothesis would perform if the data was truly pseudo-Dirac. In Figure E.1 we plot the absolute and relative errors on a SM fit of NGC 1068's spectral index, as a function of the true spectral index γ_{true}



SUPPL. FIG. D.1. $LLH(\text{data}|\delta m^2) - LLH(\text{data}|\delta m_{\text{true}}^2)$, where the data was simulated as pseudo-Dirac neutrinos from NGC 1068, and 30% log-energy resolution. The injected values of the mass splittings, δm_{true}^2 are plotted as dashed vertical lines.

and the value of the uniform pseudo-Dirac mass splitting δm^2 . In this study we again assume near-perfect energy reconstruction.



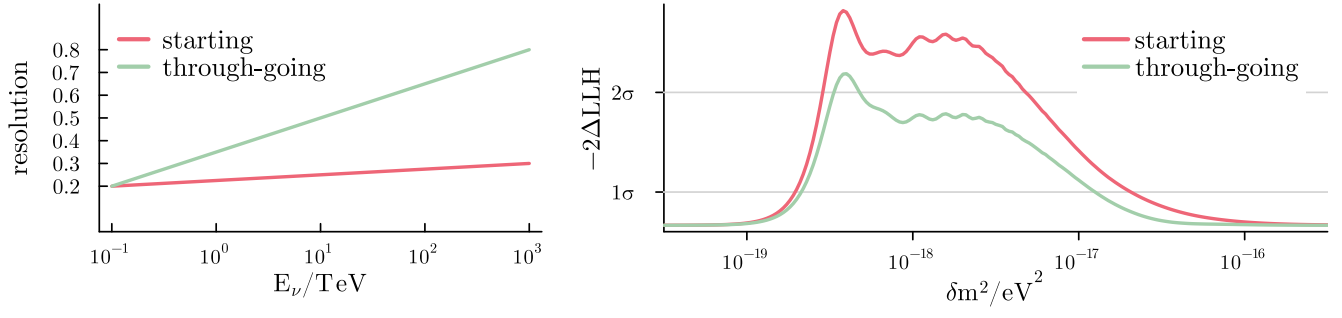
SUPPL. FIG. E.1. Absolute (*left*) and relative (*right*) error of a fit of NGC 1068's spectral index, where the data has been simulated according to a pseudo-Dirac prediction, but the fit is performed assuming a SM hypothesis.

In our binned likelihood analysis, each value of δm^2 results in a deficit of events in some combination of energy bins. Depending on the value of the spectral index, the SM hypothesis may or may not predict many events in those bins, which means the deficit may or may not be significant. If a significant number of events go missing in low energy bins, the SM hypothesis will overfit the spectral index, preferring a flatter distribution. Conversely, if a significant number of events go missing in high energy bins, the spectral index best fit value will underestimate the true value.

Appendix F: Sensitivity for starting and through-going tracks

Reconstruction algorithms struggle to estimate how much energy a muon track deposited outside of the detector volume, resulting in systematic underestimation of the true event energies [52, 71]. This problem is less significant when considering only the sub-sample of starting tracks, whose interaction vertex is contained within the detector. Reconstruction algorithms designed specifically for starting tracks can therefore achieve significantly better performance, especially at high energies.

In this subsection we consider the sensitivity that can be achieved if all the event have through-going or starting resolution. We model each resolution as a simple linear function [72], and calculate the sensitivity using NGC 1068 as the source. The models and the resulting sensitivity curves are shown in Figure F.1. In the case in which we assume all events have starting-quality resolution, the sensitivity performance is similar to the 20% curve in Figure B.1, while the through-going case is more similar to 30%.



SUPPL. FIG. F.1. *Left:* The linear models for the energy resolution of starting and through-going events as a function of energy. *Right:* Sensitivity to the pseudo-Dirac parameter space, assuming all events have starting or through-going resolution.